GEOPHYSICS, VOL. 86, NO. 5 (SEPTEMBER-OCTOBER 2021); P. WC41–WC54, 11 FIGS.
10.1190/GEO2020-0850.1

DOI:10.1190/geo2020-0850.1

Internal multiple elimination: Can we trust an acoustic approximation?

Christian Reinicke[1], Marcin Dukalski[2], and Kees Wapenaar[3]

ABSTRACT

Correct handling of strong elastic internal multiples remains a challenge for seismic imaging. Methods aimed at eliminating them are currently limited by monotonicity violations, a lack of a-priori knowledge about mode conversions, or unavailability of multicomponent sources and receivers for not only particle velocities but also the traction vector. Most of these challenges vanish in acoustic media such that Marchenko-equation-based methods are able, in theory, to remove multiples exactly (within a certain wavenumber-frequency band). In practice, however, when applied to (elastic) field data, mode conversions are unaccounted for. Aiming to support a recently published marine field data study, we build a representative synthetic model. For this setting, we demonstrate that mode conversions can have a substantial impact on the recovered multiple-free reflection response. Nevertheless, the images are significantly improved by acoustic multiple elimination. Moreover, after migration the imprint of elastic effects is considerably weaker and unlikely to alter the seismic interpretation.

INTRODUCTION

The subsurface offshore Middle East bears large amounts of hydrocarbons, however, their exploration and hence value, depend on reliable seismic images. The geology of *the region* is comprised of many, predominantly horizontal strata and occasional low relief structures (the exploration targets), that are buried under a water layer. As a result, the actual horizons and the imaging artifacts resulting from any of the countless multiple reflections are visually indistinguishable, making multiple suppression particularly challenging. Moreover, in such strongly and frequently scattering media, one expects internal multiples to be visible as a complex wavefield rather than individual events (O'Doherty and Anstey, 1971; Resnick et al., 1986). As a result, kinematic prediction of internal multiples followed by adaptive subtraction (e.g., Weglein et al., 1997; Jakubowicz, 1998; Ikelle, 2006) poses a high risk of primary energy damage. In contrast, Marchenko-equation-based demultiple methods attempt to handle internal multiples not only kinematically but also with correct amplitude. The demultiple step itself is often formulated either as an Amundsen (2001)-type deconvolution (van der Neut and Wapenaar, 2016), or as a multidimensional convolutional filter (Dukalski and de Vos, 2020).

Recently, there have been several attempts to study the applicability of Marchenko methods to *region*-characteristic geological settings. Elison et al. (2020) as well as Reinicke and Dukalski (2020) have shown acoustic synthetic examples where Marchenko multiple elimination suppresses multiple-induced complex interference patterns. These implementations are relatively simple as they only require a single user-defined temporal mute and there is no need to identify primaries to predict multiples. Moreover, Marchenko methods have shown to correctly handle all multiple generators simultaneously thanks to higher order term corrections. The success of this completely data-driven approach is contingent on the data being an accurate representation (in amplitude and phase) of the physical scattering processes in the subsurface.

Subsequently, Staring et al. (2020) applied acoustic Marchenko multiple elimination on marine field data acquired in the region. Unlike the acoustic synthetics, however, the field data contain mode converted events generated by scattering below the water bottom. Thus, the data are inconsistent with the acoustic scattering assumption of the used algorithm, casting some doubt over the validity of the results. In contrast to kinematically predicting and adaptively subtracting multiples, Marchenko methods rely on higher order terms to retrieve true amplitude predictions and to suppress crosstalk. This higher amplitude fidelity could potentially result in a higher sensitivity to ignoring elastic effects. To date, the validity of

Manuscript received by the Editor 2 December 2020; revised manuscript received 8 February 2021; published ahead of production 17 April 2021; published online 30 August 2021.
[1]Aramco Overseas Company B.V., Informaticalaan 6-12, 2628 ZD Delft, The Netherlands and Delft University of Technology, Department of Geoscience and Engineering, Stevinweg 1, 2628 CN Delft, The Netherlands. E-mail: chris.reinicke@aramcooverseas.com (corresponding author).
[2]Aramco Overseas Company B.V., Informaticalaan 6-12, 2628 ZD Delft, The Netherlands.
[3]Delft University of Technology, Department of Geoscience and Engineering, Stevinweg 1, 2628 CN Delft, The Netherlands.

DOI:10.1190/geo2020-0850.1

such acoustic approximation had been largely unexplored and poorly understood, with no clarity over the nature and the severity of the potential errors. To better understand the suitability of the acoustic Marchenko algorithm in the region and to validate the work of Staring et al. (2020), we conduct an *elastic* synthetic study using a region-representative 2D model based on well-log measurements. We further contrast their approach to what the fully elastic demultiple method would ideally require over its acoustic counterpart. A few simpler examples of applying an acoustic Marchenko scheme on a known elastic medium can be found in the literature (da Costa Filho et al., 2016, 2018). In our discussion, we consider three key aspects: (1) availability of multicomponent data with true amplitudes, (2) a temporal mute and (3) a monotonicity assumption.

In acoustic media, these requirements can be realistically met. The multicomponent data can be reduced to a single (compressional) mode and the temporal mute is derived from a single pseudoboundary (similarly to the mute used by van Borselen, 2002; Berkhout and Verschuur, 2005; Ikelle, 2006). The assumption (iii), monotonicity, requires "correct" temporal ordering of events (ten Kroode, 2002; Nita and Weglein, 2009). Although often satisfied, this assumption can be violated, particularly in the presence of large velocity variations and steep angles of incidence, e.g., the far-offset water bottom reflection. Evaluating the Marchenko solver with these monotonicity violations can lead to amplitude errors which can negatively impact the demultiple result (Reinicke et al., 2020). However, monotonicity violations can often be reduced using simple preprocessing tools such as dip-filtering.

For elastodynamic waves, Marchenko methods (Wapenaar and Slob, 2015; Reinicke et al., 2020) alike other notable internal demultiple methods (e.g., the elastic inverse scattering series, Coates and Weglein, 1996) encounter fundamental challenges. The requirement (1) is naturally violated by streamer acquisition, which only measures pressure (i.e., tensile stress) and in modern systems also particle velocities but not the shearing stresses. Furthermore, the temporal mute (2) generalizes to one pseudoboundary for each source-receiver combination of pressure and shear waves, which increases the dependency on the user and the knowledge of the subsurface. In contrast to the acoustic case, the requirement (3) can be easily violated due to coupling between modes with significant differences in propagation speeds (Sun and Innanen, 2019; Reinicke et al., 2020). As a result, even for small angles of incidence, elastic data can easily violate monotonicity. Contrary to the acoustic case, the monotonicity problem is typically no longer localized in the wavenumber-frequency domain and *cannot* be handled by dip discrimination.

In this work, we first summarize the theory of the Marchenko demultiple method. Second, we explain how the synthetic model is built and compare the acoustic with the marine reflection response. Third, the reflection responses are used to retrieve Marchenko multiple elimination results for structural imaging. Without further research, it is not possible to provide a meaningful amplitude-versus-offset (AVO) analysis because, to date, there is insufficient evidence that the presented acoustic Marchenko demultiple scheme preserves the true AVO behavior at the target level. Finally, the acoustic and marine results are respectively used to analyze the nature of the predicted multiples and the impact of ignoring elastic effects. Since our analysis excludes surface-related multiples, henceforth, the term multiples refers to the internal ones only.

A BRIEF THEORETICAL OVERVIEW

Data-driven demultiple methods assume consistency between the medium, the data and the algorithm, i.e., all three should be either acoustic or elastic. Violations of this consistency can lead to errors, e.g., by processing elastic data with acoustic demultiple algorithms. In a marine acquisition configuration, however, an elastic reflection response is recorded in an acoustic layer, i.e., we measure compressional data which have an imprint of elastic scattering effects that occur below the water bottom. Therefore, it remains unclear whether we should opt for an acoustic or elastic demultiple algorithm. Here, we discuss the acoustic version of the Marchenko demultiple theory used in the field data example by Staring et al. (2020) in the context of elastic waves. This discussion also highlights theoretical challenges of elastic Marchenko demultiple methods, particularly for marine data, which are ignored by the acoustic algorithm and will help to understand resulting artifacts in the numerical results. The theory section focuses on challenges and differences that occur when applying Marchenko methods in the elastic and marine cases as opposed to the acoustic one. Readers who are less familiar with Marchenko methods may find it helpful to start with the acoustic theory. As introduction to Marchenko redatuming and demultiple, we would respectively refer to the work by Wapenaar et al. (2014) and Slob et al. (2014) as well as by van der Neut and Wapenaar (2016), Elison et al. (2020), Dukalski and de Vos (2020), and Reinicke et al. (2020), in this order.

Marine acquisition

Elastodynamic wavefields in 3D laterally varying media are a function of five variables: (1) source- and (2) receiver-side field types for P-, S1- and S2-waves, their respective locations, (3) $\mathbf{x} = (x, y, z)$ and (4) $\mathbf{x}'$, as well as (5) the angular frequency ω. For our purposes, we organize these fields in 3×3 matrices in the P-S space,

$$\mathbf{D}(\mathbf{x}', \mathbf{x}, \omega) = \begin{pmatrix} D_{\mathrm{P,P}} & D_{\mathrm{P,S1}} & D_{\mathrm{P,S2}} \\ D_{\mathrm{S1,P}} & D_{\mathrm{S1,S1}} & D_{\mathrm{S1,S2}} \\ D_{\mathrm{S2,P}} & D_{\mathrm{S2,S1}} & D_{\mathrm{S2,S2}} \end{pmatrix} (\mathbf{x}', \mathbf{x}, \omega). \tag{1}$$

For example, the $D_{\mathrm{S1,P}}(\mathbf{x}', \mathbf{x}, \omega)$ component is the response to a dipole P-wave source with frequency ω at $\mathbf{x}$, recorded as an S1-wave by a monopole receiver at $\mathbf{x}'$. Moreover, wavefields are wavelet-free unless specified explicitly and the medium is lossless. In 2D space, the wavefield matrices can be reduced to 2×2 as the $D_{\mathrm{S2,S2}}$ element is decoupled.

Data-driven demultiple methods rely on temporal convolutions and correlations combined with matrix multiplications in the P-S space and summations of sources and receivers. Using detail-hiding operator notation (Berkhout, 1982; Wapenaar, 1989), products such as $\mathbf{D}_{\mathrm{A}}\mathbf{D}_{\mathrm{B}}$ represent the extrapolation of the field $\mathbf{D}_{\mathrm{B}}(\mathbf{x}'', \mathbf{x}, \omega)$ with $\mathbf{D}_{\mathrm{A}}(\mathbf{x}', \mathbf{x}'', \omega)$ according to,

$$\mathbf{D}_{\mathrm{A}}\mathbf{D}_{\mathrm{B}} = \int \mathbf{D}_{\mathrm{A}}(\mathbf{x}', \mathbf{x}'', \omega)\mathbf{D}_{\mathrm{B}}(\mathbf{x}'', \mathbf{x}, \omega)\mathrm{d}^2\mathbf{x}'', \tag{2}$$

which is evaluated for all frequencies ω and where the integrand involves matrix multiplications in the P-S space.

DOI:10.1190/geo2020-0850.1

We consider a marine acquisition with sources and receivers inside the water layer at $z_0 = 0$ m (no free surface). The water layer does not support shear-wave propagation and hence only P-waves can be injected and recorded (see illustration in Figure 1), resulting in a reflection response with a single nonzero component,

$$\mathbf{R}^{\cup}(\mathbf{x}'_0, \mathbf{x}_0, \omega) = \begin{pmatrix} R^{\cup}_{\mathrm{P,P}} & 0 & 0 \\ 0 & 0 & 0 \\ 0 & 0 & 0 \end{pmatrix} (\mathbf{x}'_0, \mathbf{x}_0, \omega). \quad (3)$$

The contributions to the $R^{\cup}_{\mathrm{P,P}}$ component include,

1) nonconverted primaries and multiples (they travel as P-waves only),
2) mode-converted primaries and multiples (they partially travel as S-waves below the water bottom),
3) head and surface waves originating from the elastic medium including the fluid-solid interface at the water bottom (e.g., for more details, see de Hoop and van der Hijden, 1984).

These three contributions are depicted in Figure 1 in green, red and purple, respectively.

We exclude head and surface waves from our analysis because the literature offers little analysis whether, or how, they are handled by demultiple methods.

Fully acoustic media (zero shear-wave velocity everywhere) on the other hand do not support S-waves. The resulting acoustic reflection response only contains nonconverted P-waves which are kinematically identical to those in the marine data (contributions 1 and partially 3). The amplitudes of these nonconverted P-waves, however, differ for acoustic and marine data. Given this difference, we use the term *marine data* in our paper exclusively to refer to elastic data.

Data-driven multiple elimination

Data-driven demultiple methods can be sensitive to differences between acoustic and marine data. This is particularly true for the amplitude-preserving Marchenko methods. Dukalski and de Vos (2020) show that Marchenko demultiple algorithms can be seen to provide higher order terms (involving more than a single correlation and convolution of windowed data) to the scheme by van Borselen (2002) and Ikelle (2006), thus, we review the two latter ones first.

Consider a pseudoboundary that separates the overburden ($z_0 < z < z_i$) from the target ($z > z_i$). Based on the corresponding primaries, the data are segmented in a shallow (s) and a deep (d) part which are respectively preserved by the disjoint mutes (complementary time windows) $\mathbf{\Theta}^{\cup}_s[\cdot]$ and $\mathbf{\Theta}^{\cup}_d[\cdot]$ with,

$$\mathbf{P} = \mathbf{\Theta}^{\cup}_s[\mathbf{P}] + \mathbf{\Theta}^{\cup}_d[\mathbf{P}]. \quad (4)$$

Here, the mute functions include the required domain transformations. Next, e.g., using van Borselen (2002), first-order multiples with two bounces below and one above the aforementioned pseudoboundary are kinematically predicted using temporal data correlation and convolution according to,

$$\mathbf{\Theta}^{\cup}_d[\mathbf{R}^{\cup}]\mathbf{\Theta}^{\cup}_s[\mathbf{R}^{\cup}]^*\mathbf{\Theta}^{\cup}_d[\mathbf{R}^{\cup}], \quad (5)$$

where the superscript * denotes complex-conjugation in the space-frequency domain $(\mathbf{x}', \mathbf{x}, \omega)$. The resulting predictions are adaptively subtracted from the input data, which bears the risk of damaging desired primaries. Moreover, this strategy is sensitive to erroneous predictions when the shallow data $\mathbf{\Theta}^{\cup}_s[\mathbf{R}^{\cup}]$ contain multiples that are correlated with the deep data $\mathbf{\Theta}^{\cup}_d[\mathbf{R}^{\cup}]$, a so-called multiple leakage. Even in acoustic media, the leakage can grow significantly with an increasing number of reflectors. In the marine case, however, the number of primaries and multiples increases drastically as the data contain converted modes (contributions 1 and 2). Hence, compared to acoustic data, there is an even higher risk for marine data of erroneous predictions and of damaging primaries via adaptive subtraction. The leakage can be reduced by using a recursive top-down approach in which the pseudoboundary is moved from shallower towards deeper levels.

Marchenko methods use higher order terms allowing them not only for kinematic but also for true-amplitude predictions of multiples. This amplitude fidelity removes the need for adaptive subtraction such that the nature of multiples is no longer restricted to individual events. Contrary to the top-down approach of lower order approximations, Marchenko methods are free of leakage such that they can handle the entire overburden at once, e.g., see the analytic example by Slob et al. (2014) or the elastic example with numerical accuracy by Reinicke et al. (2020). Nevertheless, the input data must be consistent with the scattering relations of the Marchenko algorithm (derived from the acoustic or elastic wave equation in heterogeneous media). This requirement is violated when applying acoustic Marchenko methods on marine data that contain elastic contributions (see points 1 and 2 discussed below equation 3). Attempts of marine field data applications still show seismic-like results, however, without offering any proof of correct multiple elimination (e.g., Ravasi et al., 2016; Jia et al., 2018; Mildner et al., 2019; Staring et al., 2020). Assessing the results can be challenging without a reference, especially, when multiples generate complex interference patterns dominated by specific frequencies. Such nature of the multiples is likely to be observed in field data as geological media, particularly in the region, often contain numerous

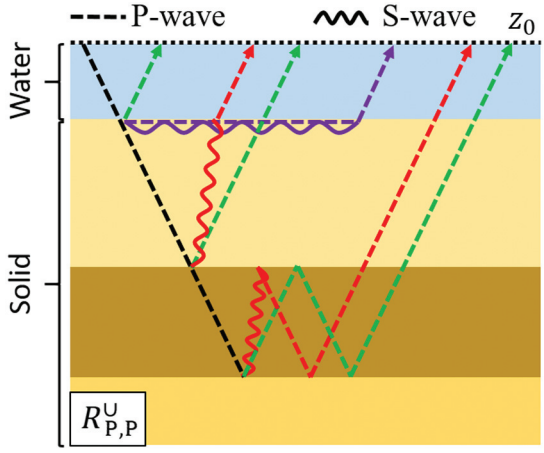

Figure 1. Illustration of the reflection response ($R^{\cup}_{\mathrm{P,P}}$ component) in a marine configuration with sources and receivers in the water layer. The acquisition level is inside an acoustic medium (water) which only supports propagation of P-waves such that S-waves are absent. However, below the water bottom the medium is elastic (solid) and thus generates primaries and multiples not only for nonconverted (green) but also for mode-converted (red) P-waves. Moreover, the reflection response can contain head and surface waves (purple).

reflectors (O'Doherty and Anstey, 1971). Hence, it is necessary to investigate on synthetic models (a) whether the nature of multiples observed in field data can be reproduced and (b) in which setting acoustic approximations produce reliable demultiple results. In this study, we carry out such complex synthetic investigation to validate the field data result by Staring et al. (2020).

(Acoustic) Marchenko demultiple theory

In the Marchenko demultiple method the key element is the dereverberation operator $\mathbf{V}(\mathbf{x}_0, \mathbf{x}'_0, \omega)$ which is used to remove multiples from the reflection response $\mathbf{R}^{\cup}$. Note that all equations in this work are derived from fundamental scattering relations and can be interpreted in the context of both acoustic and elastic waves.

Under assumptions discussed here, the dereverberation operator can be retrieved in a data-driven way through the relation,

$$\mathbf{V} = \sum_{k=0}^{\infty} \boldsymbol{\Omega}_k \quad \text{with } \boldsymbol{\Omega}_k = \boldsymbol{\Theta}_s[\boldsymbol{\Theta}_s^{\cup}[\boldsymbol{\Omega}_{k-1}\mathbf{R}^{\cup}]\mathbf{R}^{\cup *}], \tag{6}$$

as initially proposed for acoustic waves by van der Neut and Wapenaar (2016) where $\mathbf{V}$ is denoted as v^+. The series is initiated with an identity operator $\mathbf{I}$ (e.g., a band-limited delta spike at zero-offset and zero time),

$$\boldsymbol{\Omega}_0 = \mathbf{V} - \boldsymbol{\Theta}_s[\mathbf{V}] = \mathbf{I}, \tag{7}$$

and a single temporal horizon to define the mute $\boldsymbol{\Theta}_s^{\cup}[\cdot]$ (the latter is identical to van Borselen, 2002; Ikelle, 2006). Moreover, the temporal mute $\boldsymbol{\Theta}_s[\cdot]$ separates the dereverberation operator in an identity and a coda (see equation 7).

Two underlying assumptions of this strategy can be violated in the acoustic case. First, the identity and the coda can overlap in the time domain due to short-period multiples. Hence, insisting on an identity as initial value $\boldsymbol{\Omega}_0$ leads to an erroneous solution (Slob et al., 2013). Nevertheless, in some cases, the true $\mathbf{V}$ can still be recovered using additional constraints (Dukalski et al., 2019; Elison et al., 2020). Second, the function $\boldsymbol{\Theta}_s^{\cup}[\cdot]$ uses a time horizon to separate the data into a shallow and deep part which contain overburden- and target-borne primaries, respectively. This temporal separation can be accomplished only if so-called monotonicity conditions are satisfied, which we discussed recently for the elastic Marchenko demultiple method (Reinicke et al., 2020). Although monotonicity violations can also occur in acoustic media (discussed by Nita and Weglein, 2009, in the context of another demultiple algorithm), they are fortunately not an issue for reflection data of nearly 1.5D media such as the region. An exception is the water bottom reflection which is recorded after primary reflections of deeper structures at far-offsets (see offset gathers before wavenumber-frequency filtering in the section on "Application to marine data of synthetic model of the region"). In nearly 1.5D media, however, these components can be easily and inconsequentially removed during preprocessing, e.g., via dip-filtering. In the next section, we will see that the monotonicity issue is even more challenging in the elastic case.

The actual demultiple step is the so-called double dereverberation (DDR),

$$\mathbf{R}^{\cup}_{\mathrm{DDR}} = \mathbf{V}\bar{\boldsymbol{\Theta}}_d^{\cup}[\mathbf{R}^{\cup}\bar{\mathbf{V}}]. \tag{8}$$

Dukalski and de Vos (2020) show that the DDR exactly removes source- and receiver-side reverberations generated by the overburden only (i.e., primaries and peg-leg multiples, compare Figure 2a and 2b). Alternatively to the DDR in equation 8, the retrieved dereverberation operators can be used either indirectly in a multidimensional deconvolution-like equation (van der Neut and Wapenaar, 2016), or directly in a closed-formula (Dukalski and de Vos, 2020) to remove a wider class of multiples including overburden-only as well as overburden-target reverberations. The remaining target-only multiples could potentially be removed by retrieving the dereverberation operator not for a single but for a range of pseudoboundaries (analogous to the Marchenko multiple elimination schemes by Ware and Aki, 1969; Zhang et al., 2019). In terms of computational costs, however, the DDR is advantageous particularly in 3D cases because it requires neither a multi-dimensional deconvolution nor the retrieval of dereverberation operators for a range of pseudoboundaries. The dereverberation operators with and without a bar (see equation 8) act on the source- and receiver-side respectively. For sufficiently flat reflectors, the two operators are related to a very good approximation via

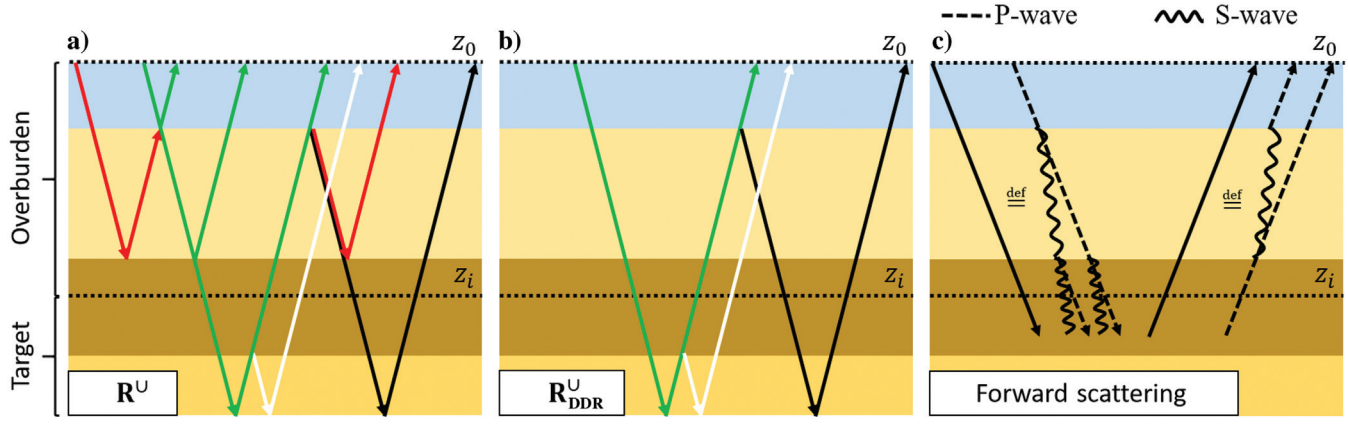

Figure 2. Illustration of different classes of multiples. (a) The reflection response $\mathbf{R}^{\cup}$ contains primaries (green) and multiples that are generated only by the overburden (red) or the target (white) or by the overburden and the target together (black). (b) DDR retrieves a reflection response $\mathbf{R}^{\cup}_{\mathrm{DDR}}$ without source- and receiver-side peg leg multiples and without overburden-borne primaries (see equation 8). For acoustic media, the solid arrows represent nonconverted P-waves. In elastic media, however, the solid arrows represent forward-scattered waves as indicated in (c).

source-receiver reciprocity which was exploited by Staring et al. (2020). For elastic waves, this approximation includes a transpose in the P-S space (superscript) T according to,

$$\mathbf{V}(\mathbf{x}_0, \mathbf{x}'_0, \omega) = \bar{\mathbf{V}}^{\mathrm{T}}(\mathbf{x}'_0, \mathbf{x}_0, \omega). \tag{9}$$

In a more general situation, the source-side operator $\bar{\mathbf{V}}$ can be retrieved analogously to equation 6, except that the reflection operator is applied on shot gathers (i.e., $\mathbf{R}^{\cup}$ acts from the left instead of the right side) and the separation functions $\bar{\boldsymbol{\Theta}}_s[\cdot]$ and $\bar{\boldsymbol{\Theta}}^{\cup}_s[\cdot]$ need to be defined for interchanged sources and receivers.

Theoretical challenges of Marchenko demultiple in the marine case

For marine data, three problems can occur in the Marchenko demultiple scheme in equations 6–8: (1) noninvertible transmissions and hence (non)existence of the dereverberation operator $\mathbf{V}$, as well as (2 and 3) challenging implementation of the separation functions (2) $\boldsymbol{\Theta}_s[\cdot]$ and (3) $\boldsymbol{\Theta}^{\cup}_s[\cdot]$.

We analyze the overburden transmissions $\mathbf{T}^{\uparrow}_s(\mathbf{x}_0, \mathbf{x}_i, \omega)$ and $\mathbf{T}^{\downarrow}_s(\mathbf{x}_i, \mathbf{x}_0, \omega)$ as their inverses can be used to define the dereverberation operator. These transmissions are associated with a shallow medium (indicated by subscript s as in equation 4) that is identical to the true one in the overburden but homogeneous below ($z > z_i$). Shear waves cannot be measured or injected in the water layer such that the transmissions reduce to,

$$\mathbf{T}^{\uparrow}_s = \begin{pmatrix} T^{\uparrow}_{\mathrm{P,P}} & T^{\uparrow}_{\mathrm{P,S1}} & T^{\uparrow}_{\mathrm{P,S2}} \\ 0 & 0 & 0 \\ 0 & 0 & 0 \end{pmatrix}, \tag{10}$$

and

$$\mathbf{T}^{\downarrow}_s = \begin{pmatrix} T^{\downarrow}_{\mathrm{P,P}} & 0 & 0 \\ T^{\downarrow}_{\mathrm{S1,P}} & 0 & 0 \\ T^{\downarrow}_{\mathrm{S2,P}} & 0 & 0 \end{pmatrix}. \tag{11}$$

Moreover, the transmissions are split in a direct part and a coda, e.g., according to,

$$\mathbf{T}^{\uparrow}_s = \mathbf{T}^{\uparrow}_{s,\mathrm{dir}} + \mathbf{T}^{\uparrow}_{s,\mathrm{coda}}. \tag{12}$$

In simple cases, the direct transmission $\mathbf{T}^{\uparrow}_{s,\mathrm{dir}}$ can be a direct wave. Its physical meaning, however, can be much more general and depends on our choice for the separation function $\boldsymbol{\Theta}_s[\cdot]$ which we will discuss subsequently.

Next, the dereverberation operator can be defined as an inverse transmission that is extrapolated by its direct part. Hence, we can write the receiver- and source-side operators respectively as,

$$\mathbf{V} = \mathbf{T}^{\uparrow}_{s,\mathrm{dir}} \mathbf{T}^{\uparrow -1}_s \tag{13}$$

and

$$\bar{\mathbf{V}} = \mathbf{T}^{\downarrow -1}_s \mathbf{T}^{\downarrow}_{s,\mathrm{dir}}. \tag{14}$$

With equations 12 and 13 it becomes clearer why the dereverberation operator $\mathbf{V}$ is an identity plus a coda (see equations 6 and 7). In the marine case, however, the definition in equations 13 and 14 is problematic because the matrices $\mathbf{T}^{\uparrow}_s$ and $\mathbf{T}^{\downarrow}_s$ are not invertible (see equations 10 and 11). To *resolve* this issue, we generalize the matrix inverse to a Moore-Penrose pseudoinverse (we still denote pseudoinverses by the superscript -1 instead of $+$ to avoid confusion with downgoing waves which are often denoted by superscript $+$). Thus, the dereverberation operators $\mathbf{V}$ and $\bar{\mathbf{V}}$ can be seen as a product of a row and a column matrix (see equations 10 and 11 and equations 13 and 14), resulting in a single nonzero element, e.g.,

$$\mathbf{V} = \mathbf{T}^{\uparrow}_{s,\mathrm{dir}} \mathbf{T}^{\uparrow -1}_s = \begin{pmatrix} V_{\mathrm{P,P}} & 0 & 0 \\ 0 & 0 & 0 \\ 0 & 0 & 0 \end{pmatrix}. \tag{15}$$

The reduction of $\mathbf{V}$ from a matrix to a scalar makes equations 6 and 8 dimensionally consistent. It remains unclear, however, whether $V_{\mathrm{P,P}}$ or another scalar filter exists that correctly removes (mode-converted) multiples according to the DDR in equation 8 or using the larger closed-form formula from Dukalski and de Vos (2020). Even if it does, it is not clear whether it is obtained by evaluating equation 6.

The second problem involves the function $\boldsymbol{\Theta}_s[\cdot]$ which ought to separate the dereverberation operator $\mathbf{V}$ into an identity $\mathbf{I}$ and a coda $\mathbf{V} - \mathbf{I}$. The explicit definition of $\boldsymbol{\Theta}_s[\cdot]$ must be consistent with our choice for the direct transmission ($\mathbf{T}^{\uparrow}_{s,\mathrm{dir}}$ and $\mathbf{T}^{\downarrow}_{s,\mathrm{dir}}$) which in turn affects the dereverberation operator (see equations 13 and 14). This mutual dependency between the separation function $\boldsymbol{\Theta}_s[\cdot]$ and the direct transmission plays a pivotal role. On the one hand, a simple direct transmission is desirable because application of the dereverberation operator removes the effect of the transmission coda $\mathbf{T}^{\uparrow}_{s,\mathrm{coda}}$ but not of its direct part $\mathbf{T}^{\uparrow}_{s,\mathrm{dir}}$ (see equations 12 and 13). On the other hand, we would like for the implementation of the separation function $\boldsymbol{\Theta}_s[\cdot]$ to require a minimum amount of prior information to keep the method data-driven. Existing implementations define the function $\boldsymbol{\Theta}_s[\cdot]$ as a temporal mute that preserves causal parts only such that the direct transmission is "chosen" implicitly. For nearly 1.5D acoustic media, the resulting direct transmission can be as simple as a direct wave (van der Neut and Wapenaar, 2016). In presence of thin layers such as in the region, however, the direct transmission can also include short-period multiples (Dukalski et al., 2019; Elison et al., 2020). For more complicated geometries as well as for elastic media, the direct transmission can generalize even further to: (a) waves that scatter without changing their vertical propagation direction as depicted in Figure 2c (also known as forward-scattered waves; Wapenaar, 2014), and (b) (fast) multiples that arrive before the direct wave (see Figure 3 in Reinicke et al., 2020). In realistic media, the remaining impact of such direct transmission could be a significant source of interference. Hence, the elastic DDR would benefit from a smarter definition of the function $\boldsymbol{\Theta}_s[\cdot]$, additional constraints, or both.

The third problem occurs because monotonicity violations are much more likely in elastic media compared to acoustic ones, particularly for large differences between the P- and S-wave velocities, c_p and c_s. This is often the case for geological media and increases the possibility of multiples "outpacing" their generating primaries (Reinicke et al., 2020). The latter work demonstrates that insisting on a simple temporal mute for the function $\boldsymbol{\Theta}^{\cup}_s[\cdot]$ can lead to an erroneous dereverberation operator. Since such artifacts are due to undesired temporal overlaps, they are expected to be more

noticeable for steeper events. The three discussed problems address fundamental questions beyond the scope of our paper but will be subject to future research.

In view of the theoretical challenges, we apply an acoustic Marchenko demultiple scheme in this paper and assess the impact of ignoring elastic effects. This analysis considers the parameter regime needed for structural imaging in nearly 1.5D media such as in the region. We hypothesize that, in this setting, forward-scattering and monotonicity violations are dominated by mode conversions which are weak for small angles of incidence, and thus, these effects can be reduced by dip- filtering. Remaining (mode-converted) forward-scattering and monotonicity violations may potentially cause artifacts when applying acoustic Marchenko demultiple schemes. For sufficiently large c_p/c_s ratios, however, these artifacts have different moveout behavior than the nonconverted P-waves, and thus, perhaps may be suppressed further during migration.

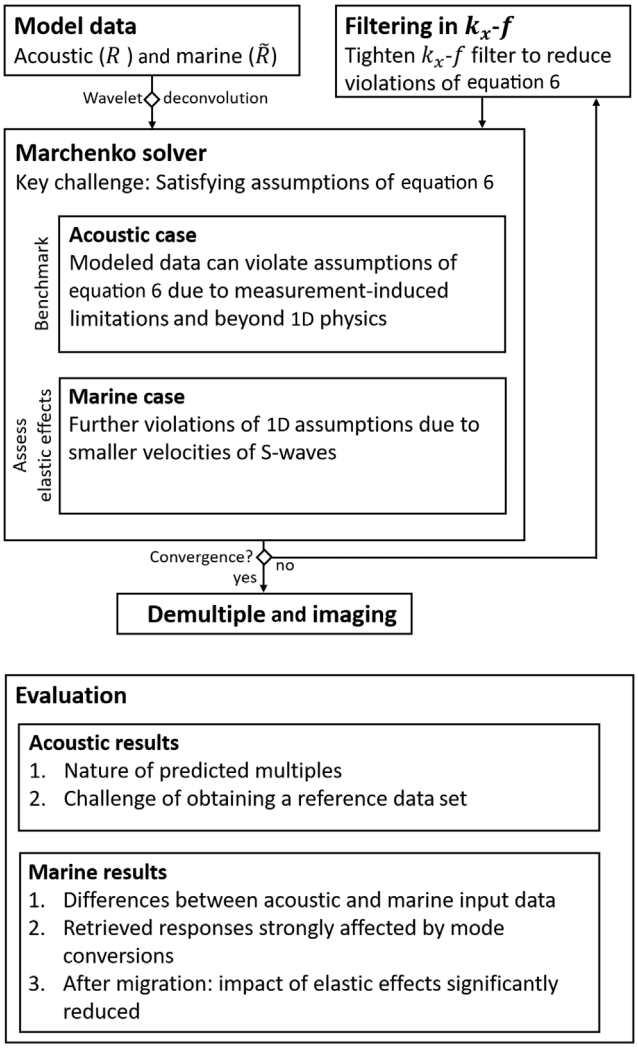

Figure 3. Overview of the synthetic experiments including (a) the processing workflow and (b) the evaluation of the results. The experiments are repeated using firstly acoustic and secondly marine reflection data. After preprocessing including wavelet deconvolution and wavenumber-frequency filtering, the acoustic data satisfies the assumptions of the Marchenko series in equation 6 to a high degree, and thus, allows us to analyze the nature of (some of) the overburden-borne multiples and serves as benchmark. The marine data, however, violates several of the aforementioned assumptions even after preprocessing, which can (and will) lead to erroneous demultiple and imaging results. The acoustic benchmark allows us to assess the properties and the severity of the errors caused by elastic effects.

Lastly, we would like to make a remark on the notation. For acoustic and marine data, all fields in equations 6–8 reduce from 3×3 matrices in the P-S space to a single (P, P) component per frequency and source/receiver location, $V_{\mathrm{P,P}}$ and $R^{\cup}_{\mathrm{P,P}}$, respectively. Thus, we use a simplified notation,

$$\begin{aligned} R^{\cup}_{\mathrm{P,P}} &\rightarrow R, \tilde{R}, \\ V_{\mathrm{P,P}} &\rightarrow V, \tilde{V}, \\ \bar{V}_{\mathrm{P,P}} &\rightarrow \bar{V}, \tilde{\bar{V}}, \\ \boldsymbol{\Theta}_{s,d}[\cdot], \boldsymbol{\Theta}^{\cup}_{s,d}[\cdot] &\rightarrow \Theta_{s,d}[\cdot], \Theta^{\cup}_{s,d}[\cdot], \\ \bar{\boldsymbol{\Theta}}_{s,d}[\cdot], \bar{\boldsymbol{\Theta}}^{\cup}_{s,d}[\cdot] &\rightarrow \bar{\Theta}_{s,d}[\cdot], \bar{\Theta}^{\cup}_{s,d}[\cdot], \end{aligned} \tag{16}$$

where fields without and with a tilde are associated with acoustic and marine data respectively.

APPLICATION TO MARINE DATA OF SYNTHETIC MODEL OF THE REGION

In this section, we want to better understand the nature of multiples and impact of elastic effects in a very realistic example. For this purpose, we conduct a synthetic study that aims to be representative for the field data example presented by Staring et al. (2020) and apply the workflow summarized in Figure 3. This processing workflow is designed for the acoustic case in which the assumptions of the Marchenko demultiple theory can be satisfied sufficiently well. Except for modeling, the marine data set is subject to identical processing steps such that we can assess the impact of ignoring elastic effects on the demultiple results.

First, acoustic and marine reflection responses are modeled using sources and receivers inside the water layer. Second, preprocessing steps are applied to closely meet the assumptions of the Marchenko series in equation 6, at least for the acoustic case. Third, the dereverberation operator is retrieved, the DDR is applied and the results are migrated. Finally, the observations made in the acoustic and the marine experiments are evaluated.

Modeling acoustic and marine reflection responses

A 2D synthetic model (x-z space) is built based on a well-log from the region including P- and S-wave velocities ($c_{\mathrm{P/S}}$) as well as densities (ρ). The model building includes four steps. First, the well-log measurements sampled at every 0.5 ft are interpolated to a regularized grid of 0.1 mm. Second, the resulting log data are band-limited according to the desired depth sampling interval Δz (10 m) and down-sampled correspondingly. Third, the well-log only provides recordings below a depth of approximately 75 m. The bathymetry is known and allows us to extrapolate the well-log for the top 25 m. For the remaining 40 m between the water bottom and the onset of the well-log, we duplicate the top 40 m that are recorded and multiply each of its entries by a random number between 0.95 and 1.05. The strength of the resulting water bottom reflection is in agreement with the field data used by Staring et al. (2020). Fourth, as the

DOI:10.1190/geo2020-0850.1

regional geology is considered to be nearly 1.5D, we include small variations of layer thicknesses, a gentle regional dip as well as minor faults and channels (see Figure 4a and 4b). For steps one to three, we observe that different parameter choices (different interpolation schemes, $\Delta z \in \{2\text{ m}, 5\text{ m}, 10\text{ m}\}$ as well as soft and hard water bottoms), lead to nearly identical reflection responses using a 30 Hz Ricker wavelet.

In this controlled experiment, acoustic and elastic reflection responses, R and $\tilde{R}$, respectively, can be modeled using the modeling tool *fdelmodc* by Thorbecke and Draganov (2011). Since the presented theory excludes surface-related multiples, the reflection data are modeled using absorbing boundary conditions. This simplification allows us to exclude potential inaccuracies due to surface-related multiple elimination from our analysis. The reflection responses are acquired at $z_0 = 0$ m inside the water layer using vertical dipole sources convolved with a 30 Hz Ricker wavelet and monopole receivers. In this experiment, we use 401 collocated sources and receivers with spatial and temporal sampling rates of $\Delta x = 12.5$ m and $\Delta t = 4$ ms, respectively. The choice of source/receiver types and sampling intervals is important because equation 6 relies on recursive wavefield extrapolations which require correctly scaled spatio-temporally unaliased data. The resulting reflection responses R and $\tilde{R}$ as well as their difference are shown in Figure 5.

Data preprocessing

Next, two preprocessing steps are applied to ensure that the data closely meet the requirements of the Marchenko demultiple method. These steps include first source wavelet deconvolution and second a wavenumber-frequency (k_x-f) filter (see k_x-f panels in Figure 5).

The second step is discussed in more detail because it can play an important, however poorly explored, role for Marchenko demultiple methods. According to the presented theory, this filter is needed to exclude wavenumber-frequency components that are associated with evanescent waves on the boundaries of the overburden at z_0 and z_i. As a side effect, at least in nearly 1.5D media, the filter removes (some of the) steeply dipping events in the offset gathers which violate monotonicity assumptions, e.g., the water bottom reflection at far offsets. An additional practical reason for wavenumber-frequency filtering, however, is to avoid divergence of equation 6, e.g., due to spatio-temporally aliasing without denser sampling. In our experience, divergence or the emergence of strong artifacts can also be caused by other effects. Hence, choosing an appropriate wavenumber-frequency support is not always straightforward. To keep the spectrum as wide as possible, increasingly narrower wavenumber-frequency filters are tested until the series in equation 6 converges reasonably well within 20 iterations (see Figure 6). The chosen wavenumber-frequency filter is defined by the velocity $c = 3.50\,\text{km s}^{-1}$ and the maximum frequency $f_{\max} = 80$ Hz.

Marchenko solver

Acoustic and marine dereverberation operators (V and $\tilde{V}$) are retrieved using 20 terms of equation 6. The separation function $\Theta_s[\cdot]$ is defined as a tapered Heaviside function $H(t - (|x_0 - x_0'|/c) - \epsilon)$ in the time domain. It removes the spatio-temporally band-limited identity with $c = 4.5\ \text{km s}^{-1}$ and a small $\epsilon > 0$ s to account for the temporal width of the source wavelet. The separation function $\Theta_s^{\cup}[\cdot]$ on the other hand applies a tapered temporal mute that removes arrivals after the two-way P-wave traveltime through the overburden. The convergence curves and the retrieved dereverberation operators are shown in Figures 6 and 7, respectively. The convergence behavior is very similar to the one observed in the complementary field data study (compare to Figure 7 in Staring et al., 2020). Furthermore, the series converges slightly faster for the marine ($\tilde{V}$) than the acoustic (V) solution. We speculate that the convergence rates of the series differ because in this case the marine reflection data contains slightly weaker nonconverted P-waves than the corresponding acoustic data.

Multiple elimination and migration

The dereverberation operator retrieval is followed by two processing steps. Firstly, the DDR is evaluated with the aim to remove peg-leg multiples, and secondly, the results are migrated.

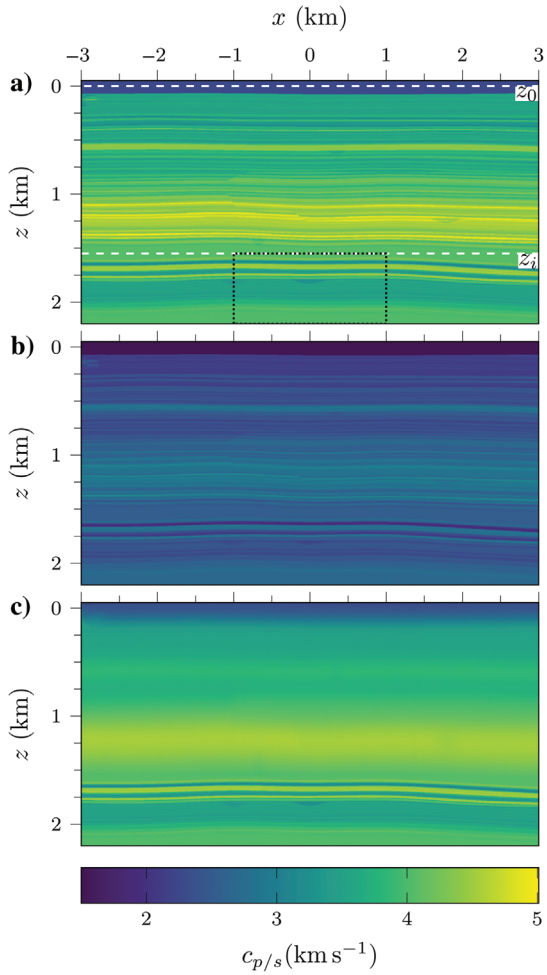

Figure 4. Synthetic model representative for the region: (a) P- and (b) S-wave velocity models. Dashed white lines indicate the recording level z_0 and the boundary between the overburden and the target at z_i. The dotted black rectangle indicates the imaging area. (c) Reference P-wave velocity model with smooth overburden. The density models are not shown but have the same geometry as the respective P-wave velocity models.

The impact of the dereverberation operator can be seen by comparing the following four quantities:

1) the late reflection response $\bar{\Theta}_d^{\cup}[R]$
2) the so-called single dereverberation (SDR) $\bar{\Theta}_d^{\cup}[R\bar{V}]$
3) the DDR $V\bar{\Theta}_d^{\cup}[R\bar{V}]$
4) the predicted multiples $R - V\bar{\Theta}_d^{\cup}[R\bar{V}]$

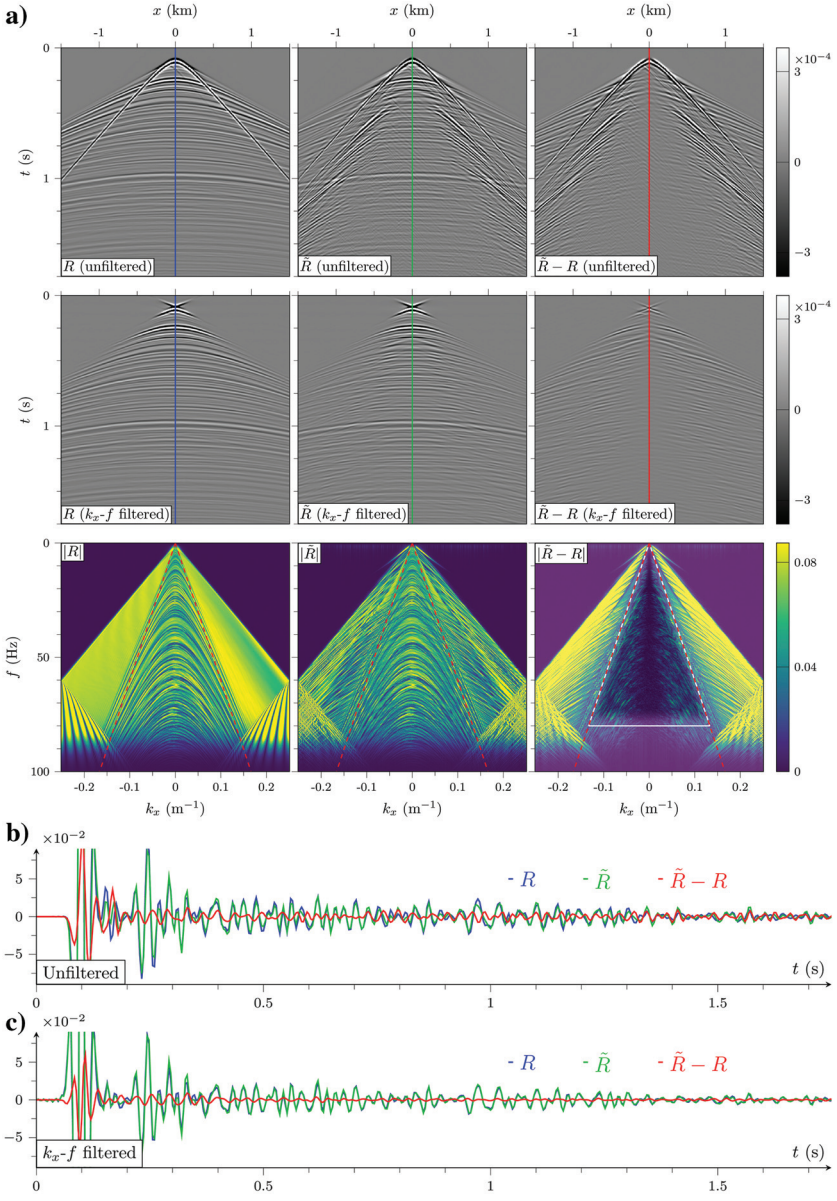

Figure 5. (a) Reflection responses of the acoustic and elastic models as well as their difference (see columns one, two and three respectively). The responses are shown before (rows one and three) and after (row two) applying a (tapered) wavenumber-frequency (k_x-f) filter, defined by $c = 3.50\ \mathrm{km\,s^{-1}}$ and $f_{\max} = 80$ Hz (indicated by the black shadow with a white outline in right-most k_x-f panel). In all figures, we show the temporal instead of the angular frequency with $f = \omega/2\pi$. Moreover, the color-coded central traces (shown in panels b and c) allow for a better amplitude comparison. The wavenumber-frequency panels show that k_x-f filtering removes the most significant differences between R and $\tilde{R}$. In the k_x-f panels, source wavelet deconvolution has been applied and red dashed lines indicate the maximum velocity on the boundaries z_0 and z_i ($c_p = 3.78\ \mathrm{km\,s^{-1}}$). The space-time and the wavenumber-frequency panels respectively are clipped at 5% and at 50% of the maximum value of the panel in the first column.

Here, the source-side dereverberation operator $\bar{V}$ is obtained using equation 9, which is a very good approximation in this case because the medium is nearly horizontally layered. For the marine case, these quantities are obtained by replacing the acoustic responses R and V with the marine ones $\tilde{R}$ and $\tilde{V}$. All of these responses are shown in the offset gathers and wavenumber-frequency spectra in Figures 8 and 9, respectively.

Next, the target reflection responses shown in Figures 8 and 9 are migrated (see Figure 10). The imaging area ($\mathbb{D}$) is restricted to the black rectangle in Figure 4a, which is shown as a magnification in Figure 10. The choice of the migration algorithm should not matter for our purposes. In this example, we use a prestack Kirchhoff depth migration (PSKDM) algorithm (e.g., Schneider, 1978), combined with a smooth velocity model. Further, a maximum offset of ± 1.6 km is considered for the migration (see dashed white lines in Figure 8). The band-limited reflectivity of the target area could be a good reference if the target were simple, velocity variations were small and the DDR aimed to remove all multiples (generated within the overburden, within the target, and between the overburden and the target). However, these conditions do not apply to the presented example, thus, the band-limited reflectivity is not shown.

Evaluation

The assumptions of the Marchenko method are closely satisfied by the preprocessed acoustic data. Thus, we first inspect the acoustic results to evaluate the nature of the predicted multiples and compare the retrieved DDR response against an approximate modeled reference (see "Acoustic results" in Figure 3). Secondly, we benchmark the marine results against the acoustic ones to analyze the impact of ignoring elastic effects and violating some of the assumptions of the Marchenko demultiple method (see "Marine results" in Figure 3).

Acoustic results

First, the impact of the DDR on acoustic data is analyzed in the offset gathers before and after migration. The retrieved dereverberation operator V is predominantly characterized by a complex interference pattern rather than individual events (see top-left panel in Figure 7a). Correspondingly, the SDR and the DDR appear to remove a significant amount of strongly interfering multiples from the input data (compare the first four panels in 8a). Here, we focus on times between $t = 1$ s and $t = 1.3$ s because this time window is used for the migration of the selected imaging area. Within this window, the SDR and DDR results reveal previously hidden arrivals

which potentially are desired primaries (see white arrows in the first three panels in Figure 8a). An analogous observation can be made in the migrated images in which the DDR uncovers structures that were originally masked by complex, potentially multiple-induced artifacts (see the first three panels in Figure 10a). There is a subtle amplitude difference between the migrated DDR result and the reference in the vicinity of $(x, z) = (0.0\text{ km}, 2.0\text{ km})$ in Figure 10. This difference is the imprint of an overburden-target multiple that is not meant to be removed by the DDR and that is not generated by the approximate reference with a smooth overburden. The overburden-target multiple can be removed by applying a deconvolution-based Marchenko demultiple scheme instead of the DDR, the respective result is shown in Fig. 6.11 of Reinicke (2020). The discussion of deconvolution-based schemes is outside of the scope of this paper, which focuses on the impact of elastic effects on the dereverberation operator recovery, rather than on how the latter is used in multiple suppression.

Second, the action of the DDR becomes very apparent in the wavenumber-frequency spectra. Here, the late reflection response $\bar{\Theta}_d^{\cup}[R]$ and the coda of the dereverberation operator $\Theta_s[V]$ have some coinciding notches and peaks (see white arrows in the respective k_x-f panels in Figures 7 and 9). When applying the SDR and DDR, the dereverberation operator partially fills the multiple-induced spectral notches of the reflection response. Furthermore, the multiples predicted by the DDR are dominated by frequencies approximately 20 and 55 Hz (see Figure 9). A similar observation is made in the field data example by Staring et al. (2020) where the predicted multiples also contain a peak around $f = 20\,\text{Hz}$ and frequencies above approximately 40 Hz were excluded.

Third, based on the above observations, we investigate whether multiple-induced imaging artifacts can be better illustrated using the spectra of the images. A detailed visual comparison of the images is challenging because they are dominated by finely layered nearly horizontal structures. Thus, we opt for an alternative analysis: A 2D spatial Fourier transformation is applied to the images $\Phi(x, z)$ in Figure 10, taking into account the selected imaging area $\mathbb{D}$ according to,

$$\Phi(k_x, k_z) = \iint_{\mathbb{D}} \Phi(x, z) e^{-i(k_x x + k_z z)} dx dz. \tag{17}$$

Next, the absolute value of the result is summed for all horizontal wavenumbers,

$$\Phi(k_z) = \sum_{k_x} |\Phi(k_x, k_z)|. \tag{18}$$

The resulting k_z-spectrum is smoother when derived from the DDR result $V\bar{\Theta}_d^{\cup}[R\bar{V}]$ instead of the late reflection response $\bar{\Theta}_d^{\cup}[R]$ (see center panel in Figure 11a). Moreover, the k_z-spectrum of the predicted multiples is dominated by two peaks approximately $k_z = 0.1\text{ m}^{-1}$ and $k_z = 0.14\text{ m}^{-1}$ (see first panel in Figure 11a). A similar nature of the predicted multiples with two characteristic low-wavenumber peaks is observed in the k_z-spectrum shown in the field data study by Staring et al. (2020).

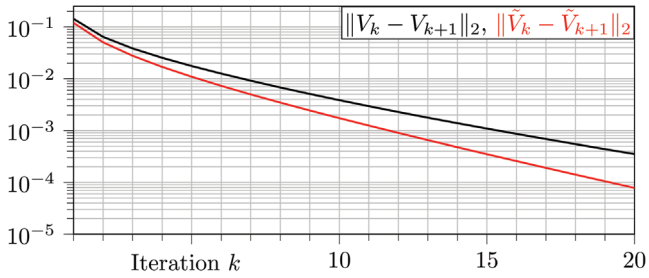

Figure 6. Convergence of the Marchenko series in equation 6 using the wavenumber-frequency filtered reflection data shown in Figure 5. The series is initiated with an identity and only updates the coda of the dereverberation operator. Therefore, the convergence is measured via the $\mathcal{L}_2$ norm of the coda update $V_k - V_{k+1}$ at each iteration $k + 1$. The black and red lines are associated with the acoustic and marine data, respectively.

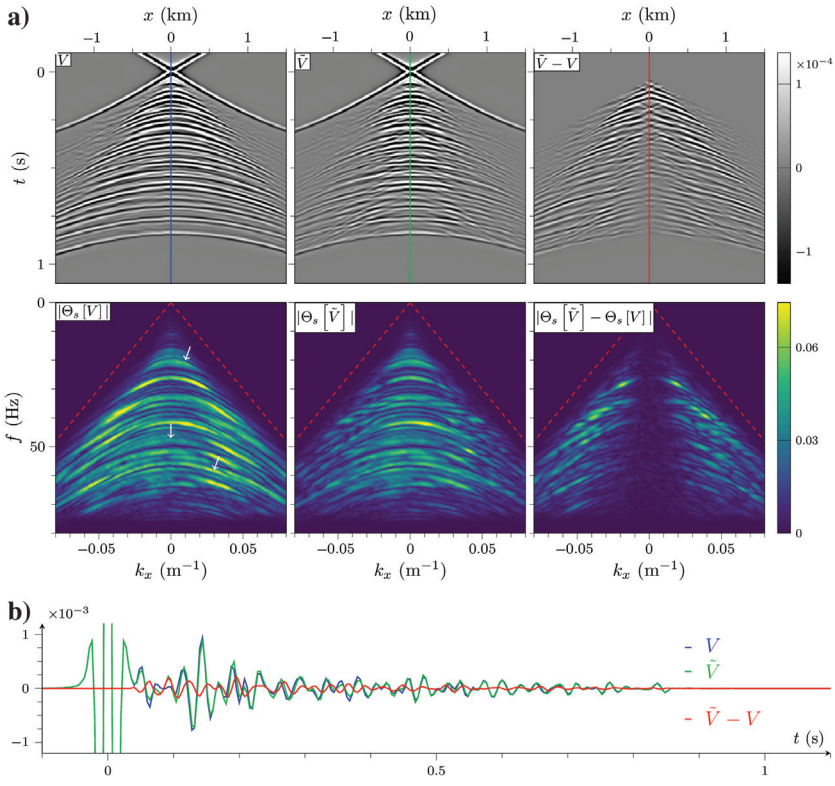

Figure 7. (a) Dereverberation operators V and $\tilde{V}$ retrieved via equation 6 using the preprocessed acoustic and marine reflection responses R and $\tilde{R}$, respectively. The x-t and k_x-f panels are respectively clipped at the 99 percentile of the panel in the first column. The amplitudes of the x-t panels can be compared easier via the color-coded central traces shown in panel b. Moreover, the k_x-f panels only show the coda of the dereverberation operator because the initial estimate (an identity) firstly is not retrieved but user-defined and secondly only adds a constant to the spectrum. The dashed red lines are associated with the same velocity as in Figure 5 ($c_p = 3.78\,\text{km s}^{-1}$) to simplify the comparison of wavenumber-frequency spectra across figures. The white arrows point to maxima in the wavenumber-frequency spectrum that, as will be shown, fill in multiple-induced notches when the DDR is applied.

Finally, an approximate reference response is modeled and compared against the DDR result. Since the model contains numerous reflectors, the multiples are expected to strongly interfere. Moreover, the predominantly horizontal layering makes it difficult to structurally discriminate between overburden-borne multiples and target primaries. Hence, a reference is needed to assess the quality of the demultiple result. For this purpose, we model a target reflection response $R^{(\mathrm{ref})}$ using an acoustic model that is identical to the true one below, z_i, but has a smooth overburden (see Figure 4c). The smoothness allows us to model scattering-free transmissions through the overburden, which excludes multiples as well as scattering-induced transmission losses. The response $R^{(\mathrm{ref})}$, however, is only an approximate reference for the DDR result and the following differences are expected. (1) Target-overburden-target multiples persist after applying the DDR demultiple method (see Figure 2a and 2b) but they are absent in the reference. (2) Contrary to the reference $R^{(\mathrm{ref})}$, the DDR result contains scattering-induced losses of the direct transmission through the actual

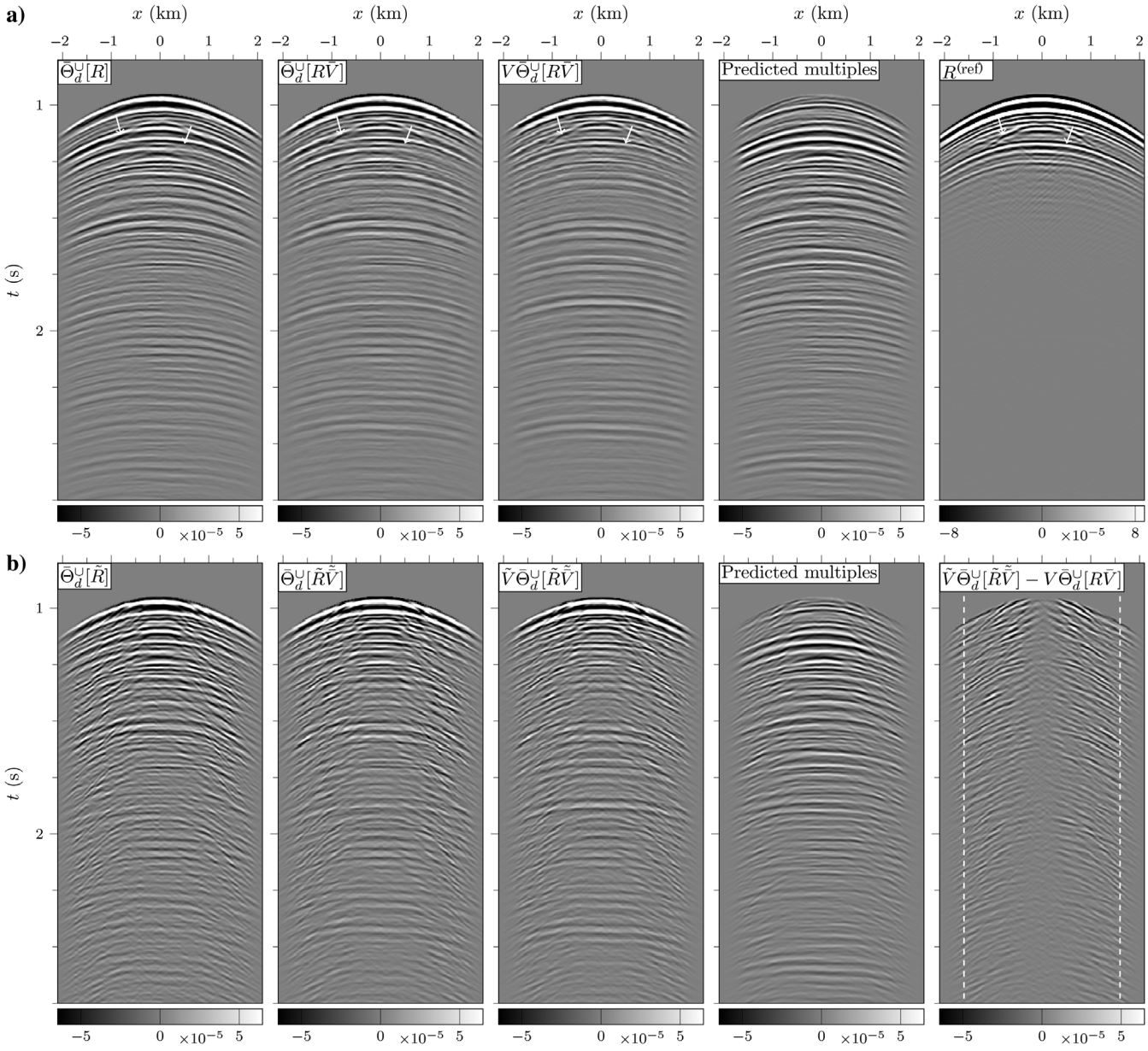

Figure 8. Target reflection responses and multiples predicted by the DDR. The target responses include late data ($\bar{\Theta}_d^{\cup}[R]$), SDR and DDR results ($\bar{\Theta}_d^{\cup}[R\bar{V}]$ and $V\bar{\Theta}_d^{\cup}[R\bar{V}]$) and the modeled reference ($R^{(\mathrm{ref})}$). The panels are retrieved from the (a) acoustic and (b) marine data, respectively. The multiples predicted by the DDR are not dominated by individual events but appear as a complicated interference pattern. The difference between the DDR results obtained from acoustic and marine data is dominated by steep events that are associated with conversions to slow propagating S-waves. The dashed white lines indicate the maximum offset that will be used for migration. Except for the modeled reference $R^{(\mathrm{ref})}$, all panels are clipped at the 99 percentile of the late acoustic data $\bar{\Theta}_d^{\cup}[R]$. As the modeled reference $R^{(\mathrm{ref})}$ does not include overburden-borne transmission losses, it is clipped independently at its 99 percentile.

overburden, i.e., these responses will have different amplitudes. (3) Imperfect smoothening of the overburden can lead to a minor global phase shift between the reference and the DDR response.

The retrieved DDR result $V\bar{\Theta}_d^{\cup}[R\bar{V}]$ indeed compares to the modeled reference $R^{(\mathrm{ref})}$ as expected. These two responses share a near-perfect kinematic match at early times (see white arrows in the respective panels in Figure 8) while they increasingly divert towards late times where more target-overburden-target multiples are expected. The SDR and DDR introduce an interference pattern at $t = 1.9$ s that is absent in the reference response (see Figure 8a). This effect could be generated by target-overburden-target multiples that are potentially suppressed in the late reflection response through destructive interference with source- and receiver-side multiples. Since recordings after about $t = 1.3$ s do not contribute to the selected imaging area, it is no surprise that the images derived from the DDR result and the reference are nearly identical (compare respective panels in Figure 10). The wavenumber-frequency and image spectra of the late reflection response and the reference differ by sharp notches (see respective panels in Figures 9 and 11). After applying the DDR, these differences are significantly reduced, indicating that the character of the observed multiples is more noticeable in these domains than in the offset gathers.

Marine results

First, the impact of elastic effects is analyzed by comparing the acoustic against the marine reflection data. The strongest

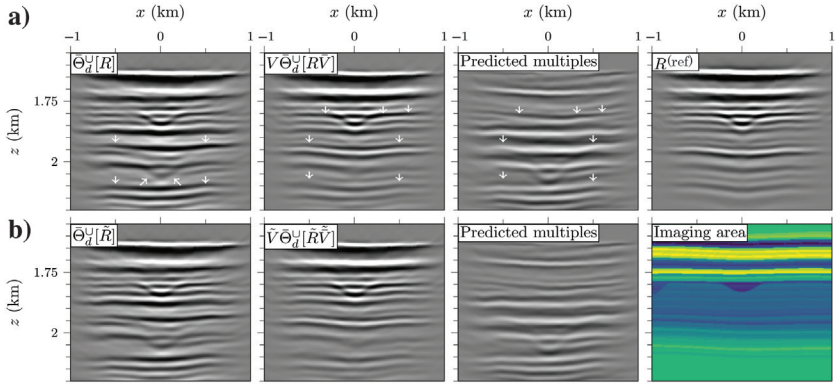

Figure 10. Images obtained from the target reflection responses in Figure 8. The images are derived from the (a) acoustic and (b) marine data, respectively. The images in each column of (a) and (b) are clipped at the 99 percentile of the respective image in (a). A magnification of c_p-model shows the imaging area. The images are computed via the PSKDM algorithm.

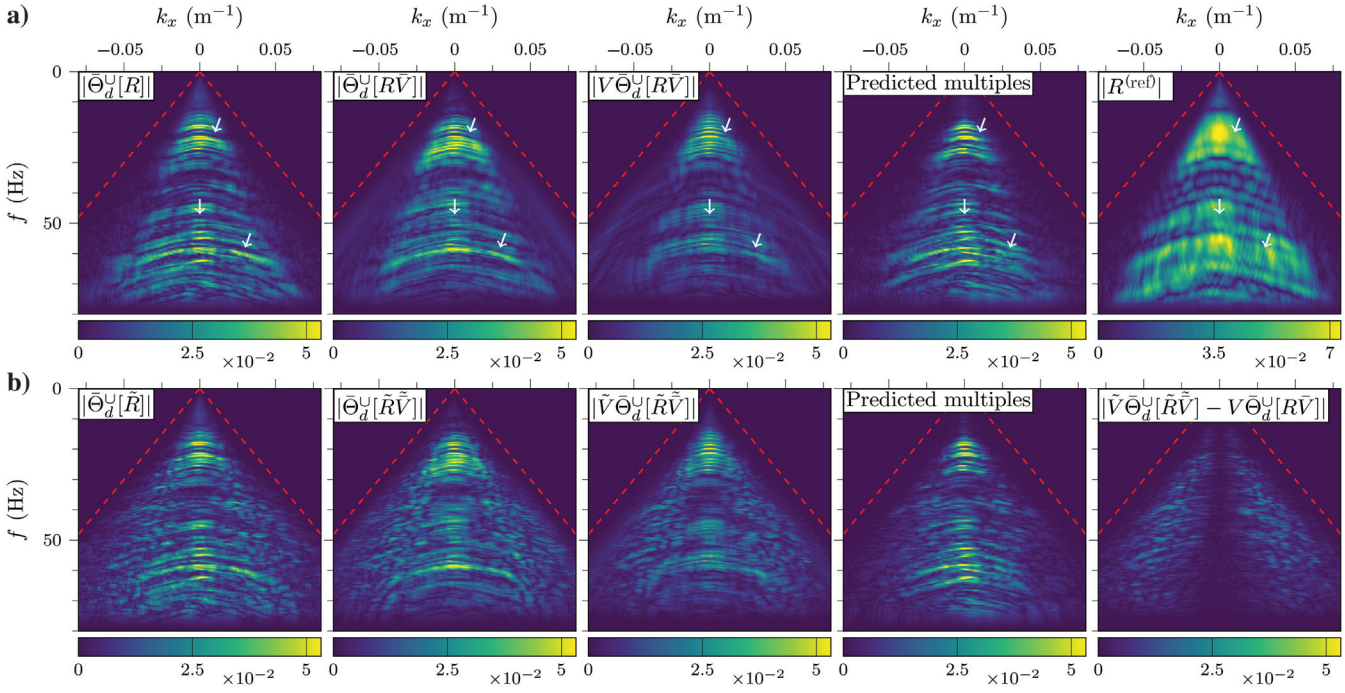

Figure 9. Similar as Figure 8 but after transformation to the wavenumber-frequency domain and source-wavelet deconvolution; the panels are retrieved from the (a) acoustic and (b) marine data, respectively. Interferences with overburden-borne multiples cause notches in the wavenumber-frequency spectrum of the late reflection response $\bar{\Theta}_d^{\cup}[R]$ which can be seen by comparing it against the reference $R^{(\mathrm{ref})}$ (see white arrows). These notches coincide with the maxima of the dereverberation operator (see white arrows in Figure 7), and are partially filled by SDR and DDR (see $\bar{\Theta}_d^{\cup}[R\bar{V}]$ and $V\bar{\Theta}_d^{\cup}[R\bar{V}]$). The wavenumber-frequency spectra of the predicted multiples also contain characteristic peaks and troughs suggesting that the multiples do not appear as individual events in the offset gathers but rather as more complicated interference patterns. The dashed red lines are associated with the same velocity as in Figure 5 ($c_p = 3.78$ km s^{-1}). Except for the modeled reference $R^{(\mathrm{ref})}$, all panels are clipped at the 99 percentile of the late acoustic data $\bar{\Theta}_d^{\cup}[R]$. As the modeled reference $R^{(\mathrm{ref})}$ does not include overburden-borne transmission losses, it is clipped independently at its 99 percentile.

differences are steep events in the offset gathers that vanish at zero offset (see top row in Figure 5a). Hence, they are likely to be associated to mode conversions to slower traveling S-waves. Furthermore, there are amplitude deviations at far-offsets, i.e., larger angles of incidence, where mode conversions tend to be stronger. Analogously, these most significant differences are found towards the outer edges of the wavenumber-frequency cone, which are removed during preprocessing (see k_x-f panels in Figure 5). Thus, the preprocessed acoustic and marine reflection operators only feature minor differences, that appear to be small variations of the AVO behavior (see right column in Figure 5a).

Second, we compare the Marchenko results obtained from acoustic and marine data prior to migration. Although some features show a high level of agreement, significant discrepancies are observed for the dereverberation operators (see right column in Figure 7a) as well as for the various target responses (compare Figure 8a and 8b and Figure 9a and 9b). These differences have a nature similar to those observed between acoustic and marine reflection data, i.e., steep events in the offset gathers. We speculate that they are caused by slower propagating mode-converted waves that are only present in the marine data.

Finally, the migration significantly reduces the differences between the acoustic and marine demultiple results (compare Figure 10a and 10b). The impact of elastic effects on the images is very subtle, which makes a detailed comparison challenging. Their k_z-spectra, however, reveal that the images derived from acoustic and marine data mostly differ around $k_z = 0.16\,\mathrm{m}^{-1}$ (indicated by vertical dashed lines in Figure 11). This difference is not introduced by the DDR algorithm but it is already present in the input data.

DISCUSSION

This synthetic case study improves our understanding of the demultiple results obtained in a recent field data example by Staring et al. (2020). Similar to other practical applications, their evaluation of the results was limited to a comparison between seismic data before and after multiple elimination. Initially, the aforementioned authors were particularly puzzled by the nearly monochromatic behavior of the predicted multiples. However, the work presented here indicates that the observed nature of multiples can indeed be expected in geological settings akin to the region. Further, our synthetic and their field data results are in near-perfect agreement on (1) the convergence behavior of the dereverberation operator retrieval and (2) the image spectra of the predicted multiples. Hence, our work provides supporting evidence for these field data results.

Our analysis focuses on structural imaging of the geology in the region, i.e., our insights may not generalize to other applications or geological settings. The consistency between acoustic Marchenko algorithms and marine reflection data decreases with increasing angles of incidence. Hence, it remains unclear whether the resulting offset-dependent amplitude variations provide reliable subsurface information, which is important, e.g., for AVO analysis or geologies beyond nearly 1.5D geometries. In particular in elastic media, the target primary will always be convolved with a train of forward-converted waves, which (a) is often ignored in AVO analysis and (b) cannot be removed within the framework of (existing) Marchenko methods without detailed prior knowledge the subsurface (Reinicke et al., 2020). For the future, it would be very valuable to conduct a synthetic study for sub-salt exploration targets where multiple elimination also remains an outstanding challenge (e.g., by including elastic effects in the synthetic salt body example by Vasconcelos et al. 2015). Moreover, our assessment excludes intrinsic attenuation which is not a first-order problem in the region. In other areas such as onshore Middle East, however, significant losses can be induced by the complex near-surface geology (Mokhtar et al., 1988). Existing Marchenko schemes that account for intrinsic attenuation unfortunately require often unavailable two-sided data including measurements above and below the target (Slob, 2016). Hence, it would be desirable to approximate and compensate for intrinsic attenuation prior to Marchenko multiple elimination which only uses single-sided illumination. Analogously to our study as well as in view of the amplitude fidelity and the higher order terms argument made prior, such approximations need to be carefully inspected using representative synthetics which will be subject to future research.

Elastic effects pose unresolved theoretical challenges for internal demultiple methods. In the context of Marchenko methods, these fundamental questions are related to the existence of the dereverberation operator as well as the implementation of the separation functions. Due to these challenges, existing field data examples apply Marchenko methods using an acoustic approximation. However, there is a high risk of drawing incorrect conclusions from the results without cautiously analyzing the impact of ignoring elastic effects. In our synthetic study, the acoustic Marchenko demultiple method appears to be robust toward elastic effects in marine data. Moreover, elastic effects present in the data before and after multiple elimination have nearly no impact on the migrated images.

Based on our experience from this project, we would like to highlight a few remarks on the implementation and theory. As for other Marchenko applications, accurate data preprocessing was crucial, yet realizable, for marine data. In this case, it was necessary to include a wavenumber-frequency filter in the preprocessing workflow

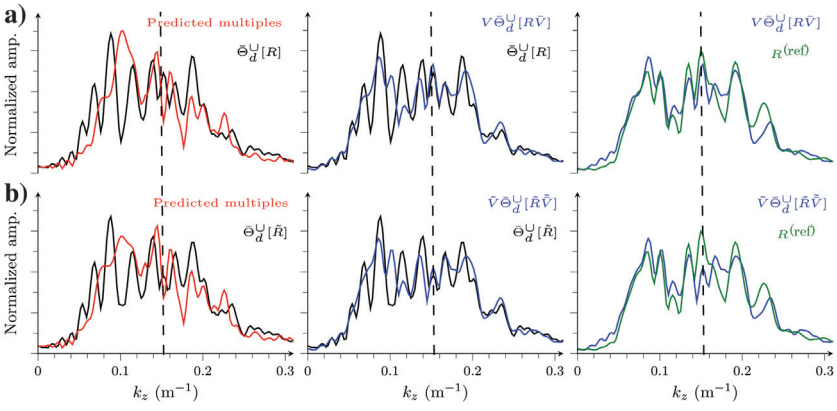

Figure 11. Vertical-wavenumber spectra of the images in Figure 10, computed according to equations 17 and 18 and associated with the (a) acoustic and (b) marine cases, respectively. A significant difference between (a) and (b) is observed at $k_z = 0.16$ m^{-1} (indicated by the vertical dashed lines).

to ensure that the assumptions of the Marchenko method are closely satisfied. We would like to emphasize that the DDR algorithm does not alter the amplitudes of the desired primaries, which facilitates the evaluation of the results. Other Marchenko demultiple methods are based on a multidimensional deconvolution, which allows them to remove a wider class of multiples, however, they do not allow for a direct comparison between the input and output data. Moreover, the presented Marchenko theory aims to remove multiples, while other Marchenko formulations additionally apply redatuming (e.g., see Wapenaar et al., 2014). The marine case is challenging for both of these strategies because the existence of the respective demultiple operators is no longer guaranteed. Multiple elimination without redatuming, however, may be easier because we can hope that an identity is still a good initial estimate for the dereverberation operator.

CONCLUSION

In the presented synthetic example, the acoustic Marchenko method appears to correctly remove acoustic multiples and seems undeterred by elastic effects. The DDR scheme uses similar operations and data as conventional internal demultiple methods but preserves true amplitudes. This advantage enables Marchenko methods to handle multiples without the need for adaptive subtraction. The nature of multiples in field data can often be very complex as, e.g., observed in the aforementioned field data application. To better understand and evaluate respective demultiple results, we found it extremely useful to conduct a representative synthetic case study. The similarities between these independently obtained results emphasize the relevance and reliability of the presented work.

ACKNOWLEDGMENTS

We thank P. Elison for support with the PSKDM software and advice. This project has significantly benefited from insightful discussion with the authors of Staring et al. (2020). The research of K. Wapenaar has received funding from the European Research Council (grant no. 742703).

DATA AND MATERIALS AVAILABILITY

Data associated with this research are confidential and cannot be released.

REFERENCES

Amundsen, L., 2001, Elimination of free-surface related multiples without need of the source wavelet: Geophysics, **66**, 327–341, doi: 10.1190/1.1444912.

Berkhout, A., 1982, Seismic migration, imaging of acoustic wave energy by wave field extrapolation: A: Theoretical aspects, 2nd ed.: Elsevier.

Berkhout, A., and D. Verschuur, 2005, Removal of internal multiples with the common-focus-point (CFP) approach — Part 1: Explanation of the theory: Geophysics, **70**, no. 3, V45–V60, doi: 10.1190/1.1925753.

Coates, R. T., and A. B. Weglein, 1996, Internal multiple attenuation using inverse scattering: Results from prestack 1 & 2D acoustic and elastic synthetics: 66th Annual International Meeting, SEG, Expanded Abstracts, 1522–1525, doi: 10.1190/1.1826408.

da Costa Filho, C. A., G. A. Meles, and A. Curtis, 2016, Elastic internal multiple prediction using Marchenko and interferometric methods: 86th Annual International Meeting, SEG, Expanded Abstracts, 4545–4549, doi: 10.1190/segam2016-13577127.1.

da Costa Filho, C. A., K. Tant, A. Curtis, A. Mulholland, and C. M. Moran, 2018, Using laboratory experiments to develop and test new Marchenko and imaging methods: 88th Annual International Meeting, SEG, Expanded Abstracts, 4352–4356, doi: 10.1190/segam2018-2979521.1.

de Hoop, A. T., and J. H. van der Hijden, 1984, Generation of acoustic waves by an impulsive point source in a fluid/solid configuration with a plane boundary: The Journal of the Acoustical Society of America, **75**, 1709–1715, doi: 10.1121/1.390970.

Dukalski, M., and K. de Vos, 2020, A closed formula for true-amplitude overburden generated interbed de-multiple: 82nd Annual International Conference and Exhibition, EAGE, Extended Abstracts, 1–5, doi: 10.3997/2214-4609.202010903.

Dukalski, M., E. Mariani, and K. de Vos, 2019, Handling short-period scattering using augmented Marchenko autofocusing: Geophysical Journal International, **216**, 2129–2133, doi: 10.1093/gji/ggy544.

Elison, P., M. S. Dukalski, K. de Vos, D.-J. van Manen, and J. O. Robertsson, 2020, Data-driven control over short-period internal multiples in media with a horizontally layered overburden: Geophysical Journal International, **221**, 769–787, doi: 10.1093/gji/ggaa020.

Ikelle, L. T., 2006, A construct of internal multiples from surface data only: The concept of virtual seismic events: Geophysical Journal International, **164**, 383–393, doi: 10.1111/j.1365-246X.2006.02857.x.

Jakubowicz, H., 1998, Wave equation prediction and removal of interbed multiples: 68th Annual International Meeting, SEG, Expanded Abstracts, 1527–1530, doi: 10.1190/1.1820204.

Jia, X., A. Guitton, and R. Snieder, 2018, A practical implementation of subsalt Marchenko imaging with a Gulf of Mexico data set: Geophysics, **83**, no. 5, S409–S419, doi: 10.1190/geo2017-0646.1.

Mildner, C., F. Broggini, C. A. da Costa Filho, and J. O. Robertsson, 2019, Source wavelet correction for practical Marchenko imaging: A sub-salt field-data example from the Gulf of Mexico: Geophysical Prospecting, **67**, 2085–2103, doi: 10.1111/1365-2478.12822.

Mokhtar, T. A., R. Herrmann, and D. Russell, 1988, Seismic velocity and Q model for the shallow structure of the Arabian shield from short-period Rayleigh waves: Geophysics, **53**, 1379–1387, doi: 10.1190/1.1442417.

Nita, B. G., and A. B. Weglein, 2009, Pseudo-depth/intercept-time monotonicity requirements in the inverse scattering algorithm for predicting internal multiple reflections: Communications in Computational Physics, **5**, 163.

O'Doherty, R., and N. A. Anstey, 1971, Reflections on amplitudes: Geophysical Prospecting, **19**, 430–458, doi: 10.1111/j.1365-2478.1971.tb00610.x.

Ravasi, M., I. Vasconcelos, A. Kritski, A. Curtis, C. A. da Costa Filho, and G. A. Meles, 2016, Target-oriented Marchenko imaging of a North Sea field: Geophysical Journal International, **205**, 99–104, doi: 10.1093/gji/ggv528.

Reinicke, C., 2020, Elastodynamic Marchenko inverse scattering: A multiple-elimination strategy for imaging of elastodynamic seismic reflection data: Ph.D. thesis, Delft University of Technology.

Reinicke, C., and M. Dukalski, 2020, Effective media theory consistent multiple elimination with Marchenko equation based methods: 82nd Annual International Conference and Exhibition, EAGE, Extended Abstracts, 1–5, doi: 10.3997/2214-4609.202010907.

Reinicke, C., M. Dukalski, and K. Wapenaar, 2020, Comparison of monotonicity challenges encountered by the inverse scattering series and the Marchenko de-multiple method for elastic waves: Geophysics, **85**, no. 5, Q11–Q26, doi: 10.1190/geo2019-0674.1.

Resnick, J., I. Lerche, and R. Shuey, 1986, Reflection, transmission, and the generalized primary wave: Geophysical Journal International, **87**, 349–377, doi: 10.1111/j.1365-246X.1986.tb06628.x.

Schneider, W. A., 1978, Integral formulation for migration in two and three dimensions: Geophysics, **43**, 49–76, doi: 10.1190/1.1440828.

Slob, E., 2016, Green's function retrieval and Marchenko imaging in a dissipative acoustic medium: Physical Review Letters, **116**, 164301, doi: 10.1103/PhysRevLett.116.164301.

Slob, E., K. Wapenaar, F. Broggini, and R. Snieder, 2013, Seismic reflector imaging while eliminating internal multiples using Marchenko-type equations: Geophysics, **78**, no. 6, 1ND–4ND, doi: 10.1190/2013-1009-TIOGEO.1.

Slob, E., K. Wapenaar, F. Broggini, and R. Snieder, 2014, Seismic reflector imaging using internal multiples with Marchenko-type equations: Geophysics, **79**, no. 2, S63–S76, doi: 10.1190/geo2013-0095.1.

Staring, M., M. Dukalski, M. Belonosov, R. Baardman, J. Yoo, R. Hegge, R. Borselen, and K. Wapenaar, 2020, R-EPSI and Marchenko equation-based workflow for multiple suppression in the case of a shallow water layer and a complex overburden: A 2D case study in the Arabian Gulf: Geophysics, **86**, no. 2, Q15–Q25, doi: 10.1190/geo2020-0204.1.

Sun, J., and K. A. Innanen, 2019, A plane-wave formulation and numerical analysis of elastic multicomponent inverse scattering series internal multiple prediction: Geophysics, **84**, no. 5, V255–V269, doi: 10.1190/geo2018-0259.1.

ten Kroode, F., 2002, Prediction of internal multiples: Wave Motion, **35**, 315–338, doi: 10.1016/S0165-2125(01)00109-3.

Thorbecke, J. W., and D. Draganov, 2011, Finite-difference modeling experiments for seismic interferometry: Geophysics, **76**, no. 6, H1–H18, doi: 10.1190/geo2010-0039.1.

van Borselen, R., 2002, Data-driven interbed multiple removal: Strategies and examples: 72nd Annual International Meeting, SEG, Expanded Abstracts, 2106–2109, doi: 10.1190/1.1817119.
van der Neut, J., and K. Wapenaar, 2016, Adaptive overburden elimination with the multidimensional Marchenko equation: Geophysics, **81**, no. 5, T265–T284, doi: 10.1190/geo2016-0024.1.
Vasconcelos, I., K. Wapenaar, J. van der Neut, C. Thomson, and M. Ravasi, 2015, Using inverse transmission matrices for Marchenko redatuming in highly complex media: 85th Annual International Meeting, SEG, Expanded Abstracts, 5081–5086, doi: 10.1190/segam2015-5896301.1.
Wapenaar, C. P. A., 1989, Elastic wave field extrapolation: Redatuming of single- and multicomponent seismic data: Elsevier.
Wapenaar, K., 2014, Single-sided Marchenko focusing of compressional and shear waves: Physical Review E, **90**, 63202, doi: 10.1103/PhysRevE.90.063202.
Wapenaar, K., and E. Slob, 2015, Initial conditions for elastodynamic Green's function retrieval by the Marchenko method: 85th Annual International Meeting, SEG, Expanded Abstracts, 5074–5080, doi: 10.1190/segam2015-5916768.1.
Wapenaar, K., J. Thorbecke, J. van der Neut, F. Broggini, E. Slob, and R. Snieder, 2014, Marchenko imaging: Geophysics, **79**, no. 3, WA39–WA57, doi: 10.1190/geo2013-0302.1.
Ware, J. A., and K. Aki, 1969, Continuous and discrete inverse-scattering problems in a stratified elastic medium — 1: Plane waves at normal incidence: The Journal of the Acoustical Society of America, **45**, 911–921, doi: 10.1121/1.1911568.
Weglein, A. B., F. A. Gasparotto, P. M. Carvalho, and R. H. Stolt, 1997, An inverse scattering series method for attenuating multiples in seismic reflection data: Geophysics, **62**, 1975–1989, doi: 10.1190/1.1444298.
Zhang, L., J. Thorbecke, K. Wapenaar, and E. Slob, 2019, Transmission compensated primary reflection retrieval in the data domain and consequences for imaging: Geophysics, **84**, no. 4, Q27–Q36, doi: 10.1190/geo2018-0340.1.

Biographies and photographs of the authors are not available.